Novel Capacitive Pressure Sensor

Ezzat G. Bakhoum, *Senior Member, IEEE*, and Marvin H. M. Cheng, *Member, IEEE*

***Abstract*—A new microelectromechanical-systems capacitive pressure sensor with extremely high sensitivity (2.24 μF/kPa) is introduced. The sensor essentially consists of a small drop of mercury and a flat aluminum electrode that are separated by a 1 μm-thick layer of Barium Strontium Titanate (a high dielectric-constant ceramic). The assembly constitutes a parallel-plate capacitor where the surface area of the electrodes is variable to a high degree. The mercury drop is pressured by a small corrugated metal diaphragm. As the electrode area of the parallel-plate capacitor varies, a total change in capacitance of more than 6 μF is obtained. [2009-0005]**

***Index Terms*—Capacitive pressure sensors, sensors.**

I. Introduction

AMONG the pressure sensors that are widely used in industry, capacitive pressure sensors [1]–[9] are particularly noteworthy. Those sensors are characterized by very low temperature hysteresis and pressure hysteresis, in addition to low power consumption. Capacitive pressure sensors, however, suffer from inherently poor resolution. A typical capacitive pressure sensor offers a total change in capacitance of only a few pico Farads, which usually necessitates the use of a sophisticated interface/compensation circuit to sense the very small variations in capacitance.

This paper introduces a new capacitive pressure sensor with extremely high resolution and sensitivity. The prototype device that was built and tested by the authors have demonstrated a change in capacitance of approximately 6.73 μF over a pressure range of 0 to 3 kPa. Its sensitivity is therefore 2.24 μF/kPa. It is substantially higher than any of the known types of capacitive pressure sensors. The first generation of this technology was recently published by the authors [1]. This manuscript describes the second generation of the technology.

The basic concept of the new device is to mechanically deform a drop of mercury that is separated from a flat aluminum electrode by a thin layer of a dielectric material, so as to form a parallel-plate capacitor where the electrode area is variable to a high degree. This principle is illustrated in Fig. 1 below.

The principle of the new device, therefore, is to create a capacitor with a variable electrode area rather than a variable inter-electrode spacing, as commonly done in the devices shown in the literature [2]–[9]. The detailed structure of the new sensor, together with the test data, are given in the following sections. Table I below lists the four most important parameters of the new sensor: sensitivity, linearity, pressure hysteresis, and temperature hysteresis, as compared to the other known types of pressure sensors.

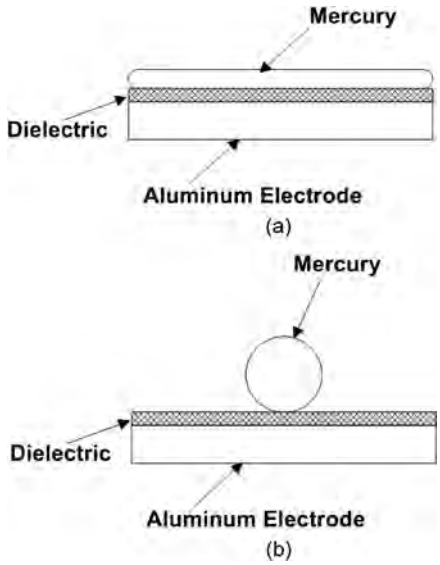

Fig. 1. (a) A drop of mercury is flattened against an aluminum electrode that is covered with a layer of a dielectric material. A parallel-plate capacitor with one liquid electrode is formed. (b) Under zero pressure, the mercury drop returns to its nearly-spherical shape. The change in capacitance between the two configurations, which is proportional to the change in the contact area of the liquid electrode, can be several hundred fold.

As the table shows, the sensitivity of the new sensor, which is verified by calculations shown further below, is substantially higher than any of the known types of pressure sensors. The hysteresis error is also substantially lower than that of other sensors. The drawback, however, is that the maximum temperature-related error is slightly worse than that of the other capacitive pressure sensors due to the thermal expansion of the mercury droplet, particularly at high temperatures. It is, however, still better than the temperature-related error offered by piezo-resistive sensors. Another important fact to mention is that while the sensor is nonlinear (like most other capacitive sensors), the equation that relates the capacitance to the applied pressure is exactly known, as will be demonstrated in the following sections.

II. Structure of the New Sensor

The basic structure of the new sensor is shown in Fig. 2. A drop of mercury with a diameter of 3 mm is placed on top of a flat aluminum electrode that is covered with a 1-μm-thick

Manuscript received January 7, 2009; revised March 28, 2010; accepted March 30, 2010. Date of publication May 3, 2010; date of current version June 3, 2010. Subject Editor J. A. Yeh.

E. G. Bakhoum is with the Department of Electrical and Computer Engineering, University of West Florida, Pensacola, FL 32514 USA (e-mail: ebakhoum@uwf.edu).

M. H. M. Cheng is with the College of Science and Technology, Georgia Southern University, Statesboro, GA 30460 USA (e-mail: hmcheng@georgiasouthern.edu).

Digital Object Identifier 10.1109/JMEMS.2010.2047632

TABLE I
COMPARISON OF THE NEW SENSOR TO THE MOST IMPORTANT TWO TYPES OF PRESSURE SENSORS: CAPACITIVE AND PIEZO-RESISTIVE (SEE [10]–[14])

	Sensitivity	Linearity	Pressure Hysteresis	Temperature Hysteresis (For temp. range of -10 °C to +80 °C)
Piezoresistive pressure sensors	Up to 25 mv/kPa	Generally linear	Up to ±1% FSO	Up to ±2% FSO
Capacitive pressure sensors	Up to 0.2 nF/kPa	Generally non-linear	Up to ±0.1% FSO	Up to ±0.5% FSO
New sensor (uncompensated)	2.24 μF/kPa	Non-linear	Less than ±0.05% FSO	Up to ±1.5% FSO

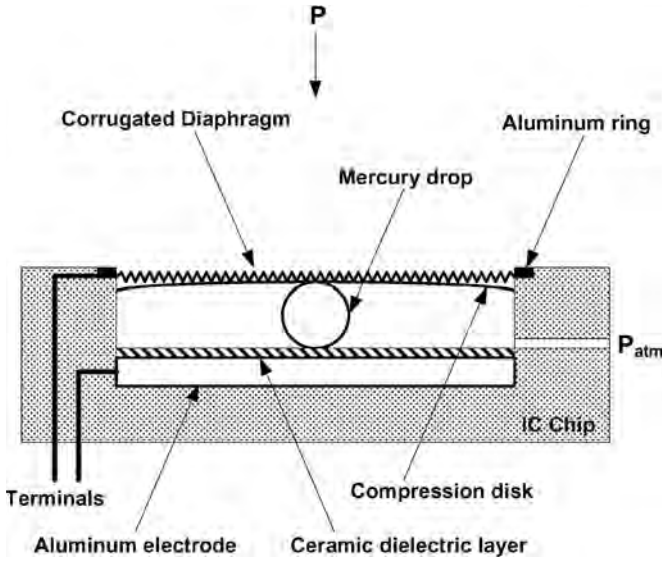

Fig. 2. Mechanical structure of the sensor (scale: 3 : 1).

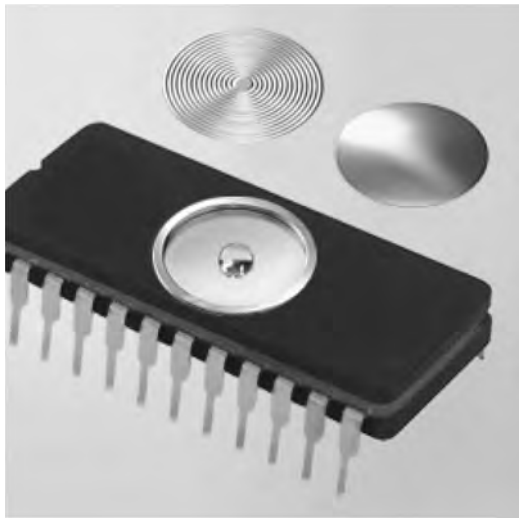

Fig. 3. Components of the sensor. The sensor is totally mounted inside a standard 24-pin DIP IC package (dimensions: 30 mm × 14 mm).

layer of a ceramic material with a very high dielectric constant (specifically, $BaSrTiO_3$, with a dielectric constant of 12 000–15 000). The drop is held in place by means of an aluminum disk that serves as the compression mechanism. The compression disk, in turn, is acted upon by means of a corrugated stainless-steel diaphragm, as shown (those corrugated diaphragms are available from a number of industrial suppliers). The compression disk is slightly curved, as shown in the figure, such that the spacing between the disk and the ceramic layer is exactly 3 mm at the center but less than 3 mm everywhere else. In this manner, the mercury drop will be forced to the center each time the stainless steel diaphragm retracts. The diaphragm is held in place by a thin aluminum ring, as shown (conductive paste between the rim of the diaphragm and the ring allows an air-tight seal to be formed). The entire assembly is mounted inside an open-cavity, 24-pin DIP IC package. A photograph of the components of the sensor is shown in Fig. 3.

Since the air that surrounds the mercury droplet must be allowed to exit from the sensor and reenter as the sensor is pressurized/depressurized, an atmospheric pressure relief conduit is drilled in the IC package, as shown on the right-hand side of Fig. 2. In most applications, that conduit will be connected to an atmospheric pressure environment via, for example, an external tube to be connected to the sensor (it will be advantageous to connect the pressure relief conduit to the ambient environment through a moisture isolation chamber in order to prevent moisture from penetrating inside the sensor). In applications where it is desired to detect pressures that are lower than the atmospheric pressure at sea level (like aircraft altitude applications, for example), a suitable vacuum can be initially applied to the pressure relief conduit (in which case, the mercury drop will be initially flattened at sea level).

Concerning the 1-μm-thick layer of $BaSrTiO_3$, it was deposited on the surface of the aluminum electrode by using the electrophoretic deposition technique [15]. Fig. 4 shows a scanning electron microscope (SEM) picture of that ceramic layer deposited on the surface of the electrode. The dielectric constant of the ceramic layer was found to be approximately 12 000, as expected for this material [16], [17].

A word is now in order concerning the interface circuit used with the sensor. At the present time, the interface circuit used is a 555 timer working in an oscillator mode, essentially for converting the capacitance to frequency. Such a circuit is very well known in the literature, and is described in references such as [18]. The equation that characterizes the 555 oscillator is $(1-\exp[-1/2fRC])=2/3$ [18]. Given a known resistance R, the value of the unknown capacitance C can be easily calculated from that equation by observing the frequency f of the

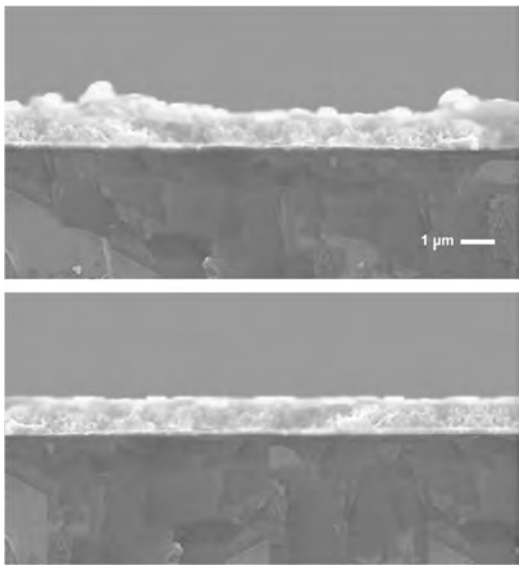

Fig. 4. SEM micrograph of the 1-μm-thick layer of $BaSrTiO_3$ deposited on the surface of the aluminum electrode (upper) and a micrograph of the same layer after fine polishing (lower).

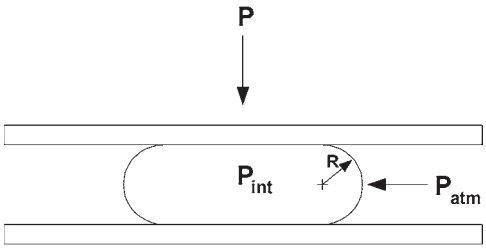

Fig. 5. Pressures and geometry in the deformation of a drop of mercury.

resulting square wave. The miniature, surface-mount 555 chip is integrated inside the open cavity package shown in Fig. 3 (the chip is mounted underneath the sensor and is not shown in the photograph). It should be pointed out that the interface circuit does not amplify or compensate for the nonlinear characteristics of the sensor (i.e., the sensor is uncompensated, as shown in Table I). The signal-to-noise ratio of the entire assembly (sensor + interface circuit) was found to be substantially high (40 dB or higher).

III. Theory of Operation

A. Pressure-Geometry Relationship in the Deformation of a Drop of Mercury

Fig. 5 shows the geometry of a drop of mercury that is deformed between two solid surfaces. The vertical pressure that is acting on the drop is P, and the lateral pressure is the atmospheric pressure $P_{\rm atm}$. $P_{\rm int}$ is the internal pressure, and R is the radius of curvature of the part of the surface of the liquid that is not flattened, as shown.

The internal pressure $P_{\rm int}$ in the liquid must be balanced by the atmospheric pressure plus the Laplace pressure, or the pressure due to surface tension [19]; that is,

$$P_{\rm int} = P_{\rm atm} + \frac{2\gamma}{R} \tag{1}$$

where $2\gamma/R$ is the Laplace pressure and γ is the surface tension of mercury. As the drop of mercury is flattened, the difference in the internal pressure will be equal to the applied pressure P, i.e.,

$$P = P_{\rm int} - (P_{\rm int})_0 \tag{2}$$

where $(P_{\rm int})_0$ is the internal pressure at zero applied pressure. By using (1), (2) can be written as follows:

$$P = P_{\rm atm} + \frac{2\gamma}{R} - \left(P_{\rm atm} + \frac{2\gamma}{R_0}\right) \tag{3}$$

where R_0 is the original unflattened radius of the drop. Hence,

$$P = 2\gamma\left(\frac{1}{R} - \frac{1}{R_0}\right). \tag{4}$$

In the sensor described here, the total pressure that is applied to the device must be equal to the pressure P, plus an additional pressure that is needed to deform the metal diaphragm. That additional pressure was determined experimentally and is discussed further below.

B. Capacitance-Geometry Relationship Between a Deformed Drop of Mercury and a Flat Electrode

The capacitance of a parallel plate capacitor is given by the well-known equation [20]

$$C = \frac{\epsilon A}{d} \tag{5}$$

where ϵ is the permittivity of the dielectric medium, A is the surface area of the electrodes, and d is the thickness of the dielectric. It should be noted from Fig. 2 that the contact area, or "wetting" area, A, of the undeformed drop of mercury is very small and that an additional capacitance [beside the one defined by (5)] exists between the metal sphere and the flat electrode, with air being the dielectric. Essentially, that parasitic capacitance can be calculated from theoretical models given in references such as [21]. That parasitic capacitance, however, is totally negligible compared to the main capacitance given by (5), due to the very high dielectric constant of the ceramic dielectric layer that exists between the electrodes (that is, the air capacitance is negligible compared to the capacitance of the ceramic). Equation (5) is, therefore, the capacitance equation that is relied upon in the present work.

The wetting area A of the deformed drop (see Fig. 5) can be calculated from the fact that the volume of the drop remains constant. The volume of the undeformed drop is equal to $4\pi R_0^3/3$, where R_0 is the radius of the undeformed drop. Calculating the wetting area of the deformed drop is a simple, but rather lengthy and uninformative exercise in geometry. We just give the result

$$A = \pi\left[\sqrt{\frac{\pi^2 R^2}{16} + \frac{2R_0^3}{3R}} - \frac{\pi}{4}R\right]^2 \tag{6}$$

where R is the radius of curvature of the part of the surface of the liquid that is not flattened (see Fig. 5). The capacitance C

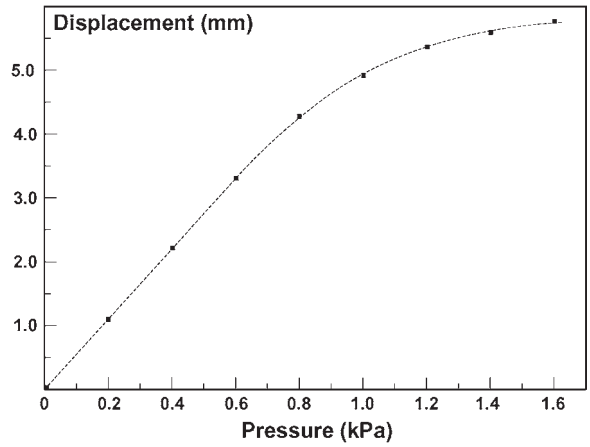

Fig. 6. Pressure-displacement relationship for the metal diaphragm used in the prototype sensor.

between the two electrodes can then be determined from (5). In the device considered here, the capacitance is actually measured, and then other parameters such as radius of curvature and pressure can be calculated from the equations. Equations (5) and (6) can be solved to give the radius of curvature R as a function of the capacitance C. This relationship is found to be

$$R = \sqrt{\frac{Cd}{\epsilon\pi^3} + \frac{4}{3}R_0^3\left(\frac{\epsilon}{\pi Cd}\right)^{1/2}} - \sqrt{\frac{Cd}{\epsilon\pi^3}}. \tag{7}$$

C. Calculation of the Pressure Acting on the Sensor

From equations (4) and (7), the pressure P acting on the mercury drop can be formulated as a function of capacitance

$$P = 2\gamma \Bigg/ \left(\sqrt{\frac{Cd}{\epsilon\pi^3} + \frac{4}{3}R_0^3\left(\frac{\epsilon}{\pi Cd}\right)^{1/2}} - \sqrt{\frac{Cd}{\epsilon\pi^3}}\right) - \frac{2\gamma}{R_0}. \tag{8}$$

The physical pressure acting on the sensor, however, is equal to P plus the pressure that is needed to deform the metal diaphragm. That additional pressure was determined experimentally. Fig. 6 shows the relationship between the pressure (in kPa) and the displacement in millimeters for the diaphragm that is used in the prototype described here.[1]

As can be seen from the figure, those diaphragms have excellent linearity in the region of small pressure. The operation of the prototype described here is actually entirely within that linear region (note, however, that this is only a part of the overall pressure acting on the sensor, and, as can be seen from (8), the sensor is actually nonlinear. More specifically, the pressure range for the diaphragm is only 0.6 kPa while the pressure range for the entire sensor, taking into account the pressure required for deforming the mercury drop, is 3 kPa). The slope of the linear relationship in Fig. 6 can be determined from the data shown. Furthermore, since the capacitance of the device is directly proportional to the displacement of the diaphragm,[2] (specifically, a displacement of 3 mm corresponds to a capacitance change from 20 nF to 6.76 μF), then, the relationship between the applied pressure and the capacitance can be easily determined as well. That relationship can be represented as

$$P_{dia} = \alpha C \tag{9}$$

where P_{dia} is the pressure acting on the diaphragm and α is the constant of proportionality. For the prototype device described here, α was found to be equal to 0.09 kPa/μF.

The physical, or total pressure acting on the sensor, is equal to the sum of the two pressures in (8) and (9). That total pressure is now finally given by

$$P_{total} = \alpha C - \frac{2\gamma}{R_0} + 2\gamma \Bigg/ \left(\sqrt{\frac{Cd}{\epsilon\pi^3} + \frac{4}{3}R_0^3\left(\frac{\epsilon}{\pi Cd}\right)^{1/2}} - \sqrt{\frac{Cd}{\epsilon\pi^3}}\right). \tag{10}$$

By knowledge of the physical parameters of the device and by measuring the capacitance between the two external electrodes, the total pressure can, therefore, be directly calculated. For the prototype sensor, the diaphragm pressure P_{dia} was found to reach a maximum of 0.6 kPa (see Fig. 6) while the pressure P required to fully deform the mercury droplet was found to be about 2.4 kPa. The sensor can, therefore, handle a total pressure of about 3 kPa. Of course, for applications where a larger pressure range is needed, a stiffer diaphragm must be used.

IV. Experimental Results

A. Basic Results

For the prototype device described here, the following are the dimensions and the physical constants:

- dielectric constant (ϵ_r) of the Barium Strontium Titanate ceramic layer: 12 000;
- thickness of the ceramic layer: 1 μm;
- radius R_0 of the undeformed mercury drop: 1.5 mm;
- wetting area of the undeformed mercury drop: 0.196 mm^2;
- wetting area of the fully deformed mercury drop: 63.6 mm^2.

Notice that the ratio between the wetting areas in the deformed and the undeformed configurations is more than 300. In fact, straightforward substitution into (5) gives capacitances of 20 nF and 6.76 μF in the two cases; and direct experimental measurements have confirmed these numbers.

Fig. 7 below shows a plot of the total pressure calculated from (10) as a function of the capacitance C, along with the actual pressure that was measured in a pressure chamber (five different samples were tested, and the readings for the five samples were essentially the same).

[1]The diaphragm was mounted on a special fixture with a transducer that measures displacement. The fixture was then tested inside a pressure chamber, as discussed later in Section IV-A.

[2]Note from (5) that C is proportional to the contact area A only since both ϵ and the dielectric thickness d are constants. A, in turn, is linearly related to the displacement of the diaphragm since the volume of the mercury drop remains constant.

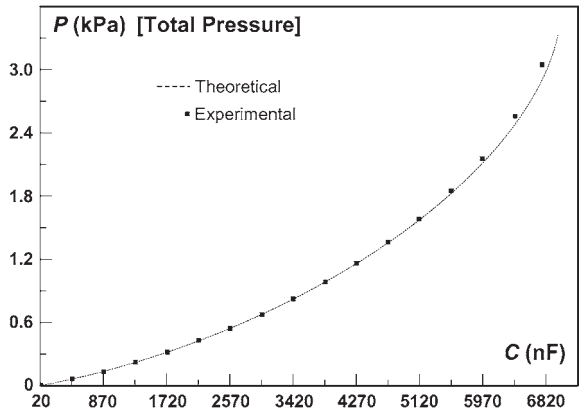

Fig. 7. Total pressure acting on the sensor as a function of the measured capacitance.

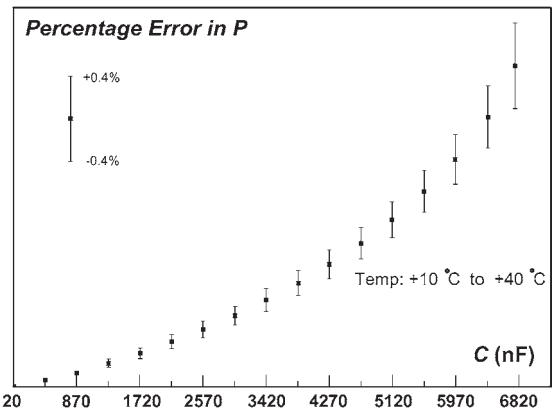

Fig. 8. Ratio $\Delta P/P$ (expressed as a percentage, with an arbitrary scale) for each of the values of the nominal pressure shown in Fig. 7. The error is the result of a maximum deviation of ± 15 °C from room temperature.

The measurements were performed in a commercial-quality pressure chamber[3] that is pressurized with compressed air (room air). The chamber is equipped with two different types of commercially available, pre-calibrated pressure sensors[4] to eliminate any possibility for errors in the measurements. The capacitance was measured directly with a capacitance meter that was connected to the sensor to eliminate any possibility for errors in the estimation of capacitance. As the graphs in Fig. 7 show, the agreement between the experimental and the theoretically calculated values of the pressure was excellent in the region of low pressures. However, a discrepancy of approximately 3% was observed in the region of high pressure (2–3 kPa). Since the discrepancy is not the result of measurement errors, the basic theoretical model of (10) will have to be refined. More specifically, it should be noted that the relationship between the displacement and the pressure acting on the diaphragm in Fig. 6 is, in fact, not perfectly linear in the operating region of 0–0.6 kPa; hence, a polynomial representation must be used instead of the simple constant α in (9). This refinement will not be given here, however, as such a polynomial relationship is strongly a function of the diaphragm used in the sensor (such a polynomial will vary depending on the type of metal, size, and structure of the diaphragm used). Alternatively, a calibration curve for the sensor can simply be used.

B. Temperature-Related Errors

For large changes in temperature, the error in the calculated pressure for the present sensor is actually slightly higher than other known types of capacitive pressure sensors due to the thermal expansion of the drop of mercury. The linear expansion of any metal object is given by [22]

$$L = L_0(1 + \lambda \Delta T) \tag{11}$$

where L is any linear dimension, λ is the metal's expansion coefficient, and ΔT is the change in temperature. The expansion in volume will, therefore, be given by

$$V = L^3 = L_0^3(1 + 3\lambda\Delta T + 3\lambda^2\Delta T^2 + \lambda^3\Delta T^3). \tag{12}$$

The coefficient of thermal expansion for mercury has a value of 9.1×10^{-5} °C^{-1}. Therefore, terms containing λ^2 and higher powers can be easily neglected. The above equation then takes the more simplified form

$$V \approx V_0(1 + 3\lambda\Delta T). \tag{13}$$

To relate (13) to the expansion of the radius R of the mercury droplet, the equation can be written as follows:

$$\frac{\Delta V}{V_0} = \frac{(\Delta R)^3}{R_0^3} = 3\lambda\Delta T. \tag{14}$$

The volume of the deformed droplet is approximately equal to area $\times$ thickness (see Fig. 5). Hence, for any specific deformation (where the thickness is held constant), the change in the contact area ΔA can be represented as follows:

$$\frac{\Delta A}{A} = \frac{(\Delta R)^3}{R_0^3} = 3\lambda\Delta T. \tag{15}$$

Furthermore, the ratio $\Delta A/A$ is equal to $\Delta C/C$, and from Fig. 7, it is clear that very small variations in capacitance can be approximated as a linear function of the pressure variation; hence,

$$\frac{\Delta A}{A} = \frac{\Delta C}{C} \approx \frac{\Delta P}{P} = 3\lambda\Delta T. \tag{16}$$

Straightforward substitution into the equation at $T = 80$ °C ($\Delta T = 55$ °C, by comparison with room temperature) gives a ratio $\Delta P/P$ of 0.015, or 1.5%. Another substitution for $T = 40$ °C ($\Delta T = 15$ °C) gives $\Delta P/P = 0.41\%$.

Fig. 8 shows the error ΔP that was measured (as a percentage) as the temperature varied in the range of $+10$ °C to $+40$ °C for each of the values of the pressure shown in Fig. 7. As shown, the maximum deviation observed was indeed 0.4%, in very good agreement with the theoretical prediction. A similar set of measurements for the temperature range of -10 °C to $+80$ °C confirmed the theoretical prediction of a maximum deviation

[3]Chamber type 175–10000 from Allied High Tech Products, Inc.

[4]61CP Series Ceramic Capacitive Pressure Sensor from Sensata Technologies, Inc. and a MAX1450 evaluation kit with a GE NovaSensor pressure sensor from Maxim Integrated Circuits, Inc.

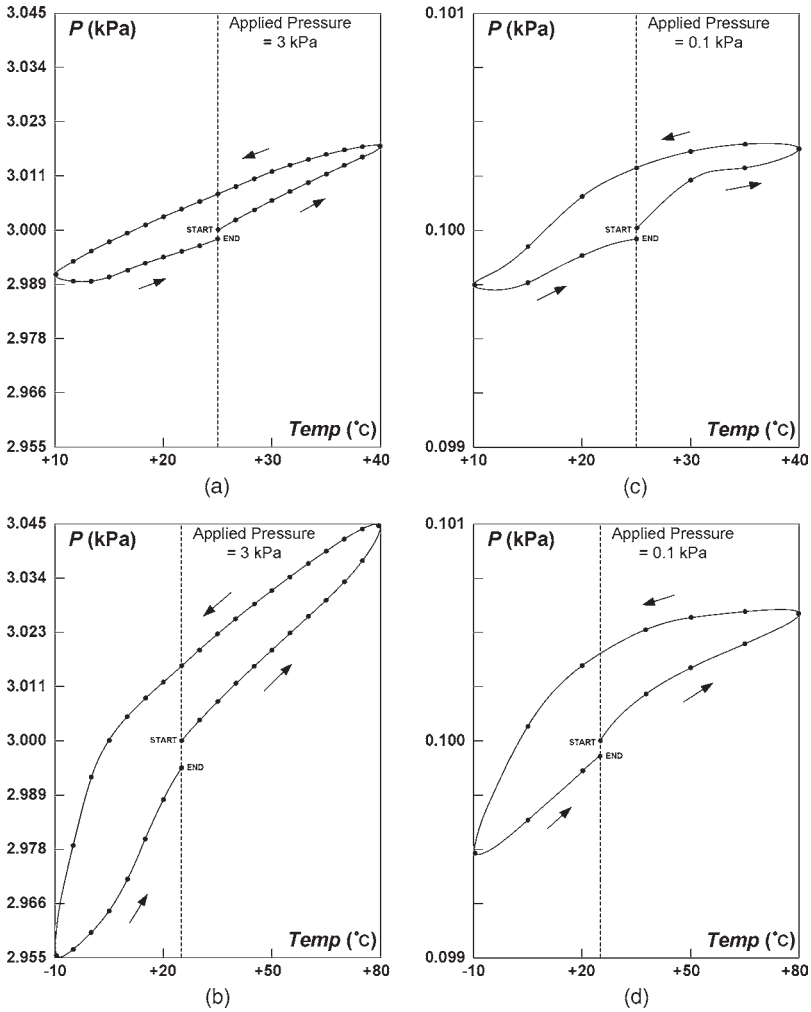

Fig. 9. Measured pressure versus temperature for a fixed applied pressure of 3 kPa [(a), (b)] and for a fixed applied pressure of 0.1 kPa [(c), (d)]. Each figure shows one complete cycle, starting at 25 °C.

$\Delta P/P$ of 1.5%. Fig. 9 shows temperature hysteresis curves that were obtained at a fixed pressure of 3 kPa (a, b), and at a fixed pressure of 0.1 kPa (c, d). The figures show the pressure that was measured as the temperature was cycled. They essentially confirm the same results.

It is very important to point out that it is possible to totally compensate for the error in the measured pressure by using (16), if the temperature is known. Finally, it is important to point out that the effects discussed above are totally due to the thermal expansion of the drop of mercury. The stainless steel diaphragm used in the sensor has a very low expansion coefficient and its contribution to the error in the value of P was found to be negligible.

C. Pressure Hysteresis

The hysteresis in the values of the calculated pressure was determined by cycling the pressure at a fixed temperature and plotting the measured pressure versus the actual applied pressure. The results are shown in Fig. 10 for two different extreme values of temperature.

As the plots in Fig. 10 show, The maximum hysteresis was found to be $\pm 0.05\%$, which is essentially negligible. (It is to be pointed out that the sensor was subjected to 1000 pressure cycles in each test, and the results did not vary significantly.)

D. Susceptibility to Mechanical Shocks

If the sensor is shocked, the mercury drop will be momentarily displaced (especially if a small pressure is acting on the drop), and it was observed that a "recovery time" is needed for the drop to return to its original position (and hence, for the momentary error to disappear). The sensor was tested on a standard electrodynamic shaker[5] that provides shock pulses of a magnitude of 34 g and a duration of 10 ms [23]. To determine the recovery time that is needed for the error to disappear after the shock, the frequency of the built-in 555 oscillator was monitored with a digital storage oscilloscope. The nominal frequency (the frequency before the shock) was noted, and the time duration that lapsed from the onset of the shock until the frequency returned to its nominal value was observed on the scope. The results of that test are shown in Fig. 11. As the figure shows, the recovery time was negligible for large pressures. This indicates that the mercury drop does

[5]Model DSS-M10, from Dynamic Solutions, Inc.

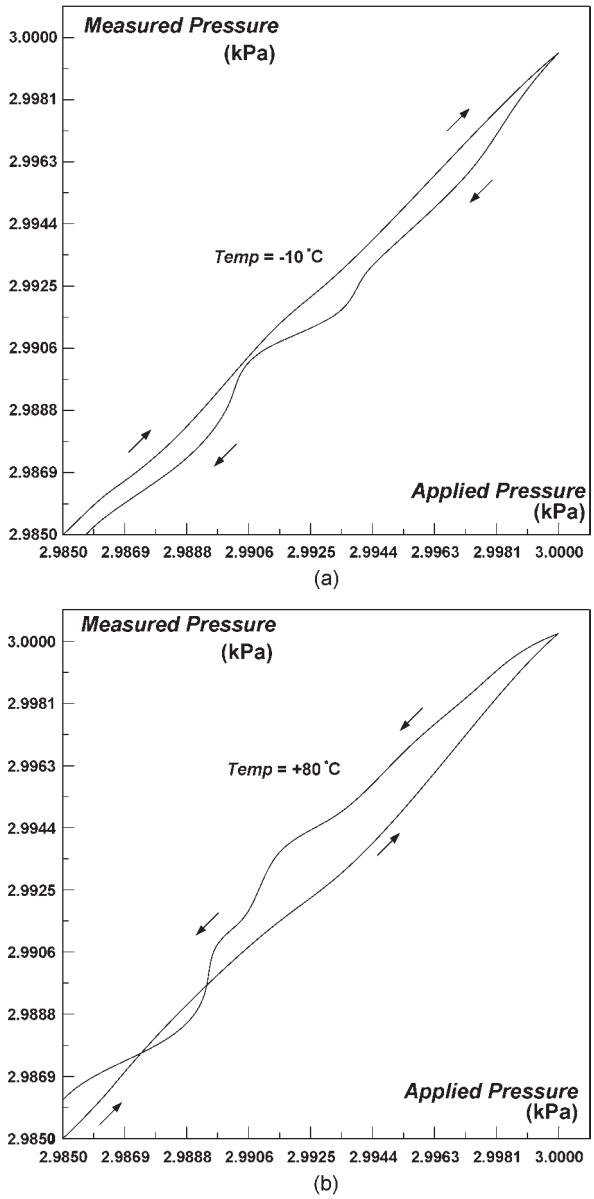

Fig. 10. Pressure hysteresis curves at -10 °C and $+80$ °C in the vicinity of the full-scale pressure (3 kPa). The maximum hysteresis error is less than $\pm 0.05\%$ FSO.

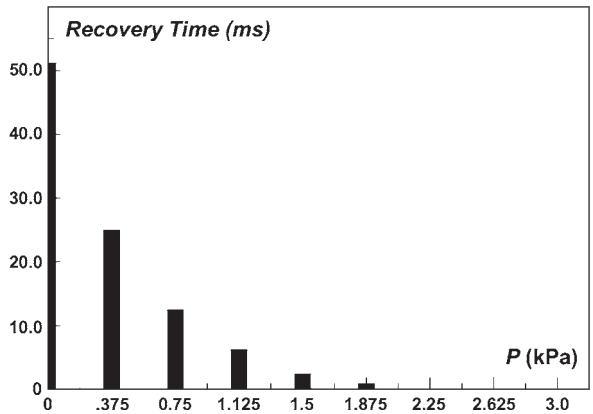

Fig. 11. After-shock recovery time as a function of the applied pressure.

not suffer from significant displacements when it is pressurized. When the pressure acting on the sensor is small, however, the recovery time is much more significant, as the figure shows. The largest recovery time observed was about 50 ms. Finally, it should be mentioned that while the sensor was mounted on the electrodynamic shaker, it was pressurized with a small mechanical fixture that uses a screw for exerting force on the steel diaphragm. By measuring the capacitance of the sensor, the pressure in each phase of the test was determined precisely.

E. Environmental Effects

At elevated temperatures (a few hundred °C), mercury reacts with the oxygen in the air to form mercury oxide. The presence of mercury oxide can severely degrade the performance of the sensor. For this reason, the sensor is not intended to function at elevated temperatures. (Another issue to consider is the expansion of the mercury drop as indicated above). Generally, the use of this sensor at temperatures above $+80$ °C is not recommended.

V. Conclusion

The new capacitive pressure sensor described in this paper has a sensitivity that is substantially higher than any of the other capacitive pressure sensors known at the present time. The prototype devices that were fabricated and tested have exhibited a change in capacitance of more than 6 μF over a pressure range of 0 to 3 kPa (the sensitivity/resolution of the sensor is, therefore, 2.24 μF/kPa). As described above, the pressure range that the sensor can handle can be increased by simply using a stiffer diaphragm. The equations that relate the applied pressure to the measured capacitance of the device are fairly simple, and testing has shown a very good agreement between theory and experiment.

References

[1] E. G. Bakhoum and M. H. M. Cheng, "Capacitive pressure sensor with very large dynamic range," *IEEE Trans. Compon. Packag. Technol.*, vol. 33, no. 1, pp. 79–83, Mar. 2010.

[2] C. S. Sander, J. W. Knutti, and J. D. Meindl, "A monolithic capacitive pressure sensor with pulse-period output," *IEEE Trans. Electron Devices*, vol. ED-27, no. 5, pp. 927–930, May 1980.

[3] H. Chau and K. D. Wise, "An ultraminiature solid state pressure sensor for a cardiovascular catheter," *IEEE Trans. Electron Devices*, vol. 35, no. 12, pp. 2355–2362, Dec. 1988.

[4] A. Yasukawa, M. Shimazoe, and Y. Matsuoka, "Simulation of circular silicon pressure sensors with a center boss for very low pressure measurement," *IEEE Trans. Electron Devices*, vol. 36, no. 7, pp. 1295–1302, Jul. 1989.

[5] J. T. Kung and H. S. Lee, "An integrated air-gap capacitor pressure sensor and digital readout with sub-100 attofarad resolution," *J. Microelectromech. Syst.*, vol. 1, no. 3, pp. 121–129, Sep. 1992.

[6] C. H. Mastrangelo, X. Zhang, and W. C. Tang, "Surface micromachined capacitive differential pressure sensor with lithographically defined silicon diaphragm," *J. Microelectromech. Syst.*, vol. 5, no. 2, pp. 98–105, Jun. 1996.

[7] A. V. Chavan and K. D. Wise, "Batch-processed vacuum-sealed capacitive pressure sensors," *J. Microelectromech. Syst.*, vol. 10, no. 4, pp. 580–588, Dec. 2001.

[8] M. X. Zhou, Q. A. Huang, M. Quin, and W. Zhou, "A novel capacitive pressure sensor based on sandwich structures," *J. Microelectromech. Syst.*, vol. 14, no. 6, pp. 1272–1282, Dec. 2005.

[9] J. N. Palasagaram and R. Ramadoss, "MEMS capacitive pressure sensor fabricated using printed circuit processing techniques," *IEEE Sensors J.*, vol. 6, no. 6, pp. 1374–1375, Dec. 2006.
[10] S. A. Dyer, *Survey of Instrumentation and Measurement*. New York: Wiley, 2001.
[11] W. C. Dunn, *Fundamentals of Industrial Instrumentation and Process Control*. Boston, MA: Artech House, 2005.
[12] *Pressure Sensors*, Kavlico Corp., Moorpark, CA, 2009. [Online]. Available: http://www.kavlico.com/products/transportation/pressure.php
[13] *SM5470 Pressure Transducers*, Servoflo Corp., Lexington, MA, 2009. [Online]. Available: http://www.servoflo.com/pressure-sensor-overview/servoflo-pressure-sensors/smi-pressure-sensors/sm5470.html
[14] *Capacitive Pressure Sensors*, Setra Corp., Boxborough, MA, 2009. [Online]. Available: http://www.setra.com/tra/pro/pdf/264.pdf
[15] O. O. Van der Biest and L. J. Vandeperre, "Electrophoretic deposition of materials," *Annu. Rev. Mater. Sci.*, vol. 29, pp. 327–352, 1999.
[16] T. Remmel, M. Schulberg, S. Fujimura, H. Honma, H. Kobayashi, H. Kohno, S. Owens, R. Deslattes, and J. Pedulla, "Barium strontium titanate thin film analysis," in *Proc. Denver X-Ray Conf.—Advances in X-Ray Analysis*, 2000, vol. 43, pp. 510–518.
[17] S. Oh, J. H. Park, and J. Akedo, "Dielectric characteristics of barium strontium titanate films prepared by aerosol deposition on a Cu substrate," *IEEE Trans. Ultrason., Ferroelectr., Freq. Control*, vol. 56, no. 3, pp. 421–424, Mar. 2009.
[18] E. A. Parr, *IC 555 Projects*. London, U.K.: Babani Publishing, Ltd., 1981, p. 13.
[19] E. Matijevic and M. Borkovec, *Surface and Colloid Science*. New York: Wiley, 1969.
[20] W. H. Hayt and J. A. Buck, *Engineering Electromagnetics*. New York: McGraw-Hill, 2006.
[21] E. Pisler and T. Adhikari, "Numerical calculation of mutual capacitance between two equal metal spheres," *Phys. Scr.*, vol. 2, no. 3, pp. 81–84, 1970.
[22] P. M. Fishbane, S. G. Gasiorowicz, and S. T. Thornton, *Physics for Scientists and Engineers*, 3rd ed. Englewood Cliffs, NJ: Prentice-Hall, 2005.
[23] C. M. Harris and A. G. Peirsol, *Shock and Vibration Handbook*. New York: McGraw-Hill, 2001.

Ezzat G. Bakhoum (SM'08) received the B.S. degree from Ain Shams University, Cairo, Egypt, in 1986, and the Master's and Ph.D. degrees from Duke University, Durham, NC, in 1989 and 1994, respectively, all in electrical engineering.

From 1994 to 1996, he was a Senior Engineer and Managing Partner at ESD Research, Inc., Research Triangle Park, NC. From 1996 to 2000, he was a Senior Engineer at Lockheed Martin/L3 Communications, Inc., Camden, NJ. From 2000 to 2005, he served as a Lecturer in the Electrical Engineering Department, New Jersey Institute of Technology, Newark. He is currently an Assistant Professor at the University of West Florida, Pensacola, FL.

Marvin H. M. Cheng (M'06) received the B.S. and M.S. degrees from National Sun Yat-sen University, Kaohsiung, Taiwan, in 1994 and 1996, respectively, and the Ph.D. degree from Purdue University, West Lafayette, IN, in 2005, all in mechanical engineering.

From 1997 to 1999, he was an R&D Engineer at the National Synchrotron Radiation Research Center in Taiwan, developing a real-time monitoring system for high-energy emission systems. Currently, he is an Assistant Professor of Mechanical Engineering Technology at Georgia Southern University, Statesboro. His current research interests include mechatronics, controller synthesis with the consideration of finite wordlength, precision, motion control, fast imaging of atomic force microscopes, and embedded controllers.